

## Toward an Iron(II) Spin-Crossover Grafted Phosphazene Polymer

Ross J. Davidson,<sup>†</sup> Eric W. Ainscough,<sup>\*,†</sup> Andrew M. Brodie,<sup>\*,†</sup> Geoffrey B. Jameson,<sup>†</sup> Mark R. Waterland,<sup>†</sup> Harry R. Allcock,<sup>‡</sup> Mark D. Hindenlang,<sup>‡</sup> Boujemaa Moubaraki,<sup>§</sup> Keith S. Murray,<sup>§</sup> Keith C. Gordon,<sup>¶</sup> Raphael Horvath,<sup>¶</sup> and Guy N. L. Jameson<sup>¶</sup>

<sup>†</sup>Chemistry—Institute of Fundamental Sciences, Massey University, Private Bag 11 222, Palmerston North 4442, New Zealand

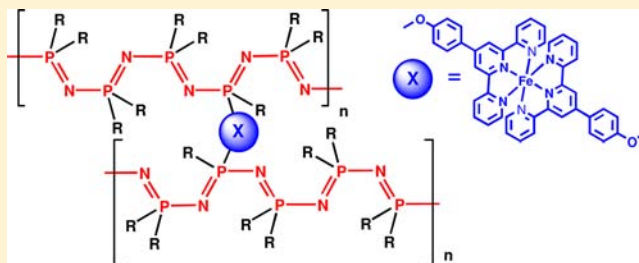
<sup>‡</sup>Department of Chemistry, The Pennsylvania State University, University Park, Pennsylvania 16802, United States

<sup>§</sup>School of Chemistry, Monash University, Building 23, Clayton, Victoria 3800, Australia

<sup>¶</sup>MacDiarmid Institute for Advanced Materials and Nanotechnology, Department of Chemistry, University of Otago, Dunedin 9016, New Zealand

### S Supporting Information

**ABSTRACT:** Two new cyclotriphosphazene ligands with pendant 2,2':6',2''-terpyridine (Terpy) moieties, namely, (pentaphenoxy){4-[2,6-bis(2-pyridyl)]pyridoxy}-cyclotriphosphazene ( $L^1$ ), (pentaphenoxy){4-[2,6-terpyridin-4-yl]phenoxy}cyclotriphosphazene ( $L^2$ ), and their respective polymeric analogues,  $L^{1P}$  and  $L^{2P}$ , were synthesized. These ligands were used to form iron(II) complexes with an  $Fe^{II}Terpy_2$  core. Variable-temperature resonance Raman, UV–visible, and Mössbauer spectroscopies with magnetic measurements aided by density functional theory calculations were used to understand the physical characteristics of the complexes. By a comparison of measurements, the polymers were shown to behave in the same way as the cyclotriphosphazene analogues. The results showed that spin crossover (SCO) can be induced to start at high temperatures by extending the spacer length of the ligand to that in  $L^2$  and  $L^{2P}$ ; this combination provides a route to forming a malleable SCO material.

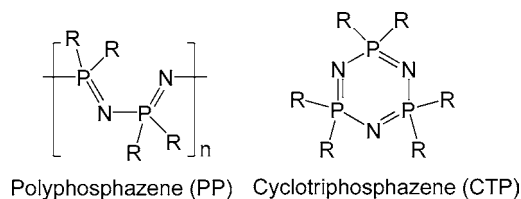


## INTRODUCTION

Spin-crossover (SCO) materials have long been heralded as having a potential use for quantum computers and massive data storage among a host of other potential applications.<sup>1,2</sup> However, one of the key difficulties in using these materials is that they are often crystalline, making deposition difficult and expensive. This has been improved by attaching long alkyl groups,<sup>3</sup> which resulted in a malleable material; however, by varying the substituents to produce suitable materials, the SCO behavior is also altered.<sup>4–6</sup> Further work was carried out by Lemaire et al. to produce an iron(III) SCO grafted polythiophene, although iron(III) is not ideal to use because each of the spin states is paramagnetic, whereas iron(II) switches from diamagnetic (low spin, LS) to paramagnetic (high spin, HS).<sup>7</sup>

Cyclo- and polyphosphazenes provide a promising solution to many of these problems. With a repeating unit of nitrogen and phosphorus atoms, they can be substituted at the phosphorus atom with two nucleophiles (see Chart 1), typically alcohols or amines. Unlike many organic polymers, it is possible to form the polymer first, e.g.,  $[NPCI_2]_n$ , followed by substitution of the chloride groups. This allows the substituents to be varied in both type and ratio. These properties have often proven to be useful in the development of ligands because coordinating substituents (pyridines, phosphines, nitriles, etc.)

### Chart 1. Generic PP and CTP Structures



can be attached to either the cyclotriphosphazene (CTP) to form discrete metal complexes<sup>8–11</sup> or polyphosphazene (PP) metallopolymers.<sup>9,12–21</sup> Previously reported polymers produced by Ainscough et al. proved that the substitution of phosphazenes with fluorophores had little effect on their physical behavior.<sup>12</sup>

This study examines the properties of iron bis(2,2':6',2''-terpyridine) ( $[Fe(Terpy)_2]^{2+}$ ) attached to both the CTP and PP platforms and measures their photo- and magnetochemical properties. A variety of techniques have been used to characterize these novel materials such as electronic absorbance, solid-state resonance Raman (rR), and Mössbauer spectroscopies as well as magnetic susceptibility. Density

Received: April 26, 2012

Published: July 10, 2012

functional theory (DFT) calculations were employed to obtain insight into the behavior of the compounds. The compounds studied were the iron(II) complexes of 2,2':6,2"-terpyridine (Terpy) and 2,6-dipyridine-2-ylpyridine-4-yl (PhTerpy). The parent Fe(Terpy)<sub>2</sub>[anion]<sub>2</sub> complexes are invariably LS at all temperatures, including "tail"-modified Terpy species.<sup>22</sup> Related iron(II) complexes of ligands similar but not identical with Terpy, viz., 2,6-bis(1*H*-benzimidazol-2-yl)pyridine, with long alkyl chains appended,<sup>23</sup> or 1,10-phenyltetrazolyl tridentate ligands, give interesting and often abrupt spin transitions.<sup>24</sup> This is the first time phosphazene systems containing these species have been reported, so it was the intent to determine whether the substitution of phosphazenes provides enough steric hindrance and the use of a phenyl spacer will alter the physical behavior of the complexes.

## EXPERIMENTAL SECTION

Analytical grades of the solvents were used, except tetrahydrofuran (THF), which was dried over an alumina column. 2,6-Bis(2-pyridyl)-4(1*H*)-pyridone (HOTerpy),<sup>25</sup> 4-(2,6-dipyridin-2-ylpyridine-4-yl)-phenol (HOPhTerpy),<sup>26</sup> 1,2,2,3,3-pentakis(phenoxy)-1-chlorocyclotriphosphazene [N<sub>3</sub>P<sub>3</sub>(OPh)<sub>5</sub>Cl],<sup>27</sup> and Ag(CH<sub>3</sub>CN)<sub>4</sub>PF<sub>6</sub><sup>28</sup> were synthesized by literature methods. [NPCL<sub>2</sub>]<sub>*n*</sub> were synthesized by the ring-opening method.<sup>29</sup> NaH (60%) dispersed in mineral oil, tetrabutylammonium bromide (TBAB), tetrabutylammonium bromide hexafluorophosphate (TBAPF<sub>6</sub>), tetrabutylammonium perchlorate (TBAClO<sub>4</sub>), 4-*tert*-butylphenol (HOPh<sup>tBu</sup>), Fe(ClO<sub>4</sub>)<sub>2</sub>·6H<sub>2</sub>O, and FeCl<sub>2</sub>·6H<sub>2</sub>O were all sourced from Aldrich. Iron-57 (95% IE) powder was obtained from Isoflex. Fe-57(ClO<sub>4</sub>)<sub>2</sub>·6H<sub>2</sub>O was produced by dissolving iron powder (200 mg, 3.5 mmol) in acetonitrile (4 mL), and perchloric acid (2.5 mL, 17.5 mmol) was added. The solution was filtered, diethyl ether was added, and the resulting solution was cooled to -4 °C, yielding pale-green crystals. The crystals were filtered and washed with diethyl ether. All manipulations were carried out under an argon atmosphere, using standard Schlenk techniques.

**Caution!** Perchlorate salts with organic ligands are potentially explosive and should be handled with the necessary precautions.

**Synthesis.** [N<sub>3</sub>P<sub>3</sub>(OPh)<sub>5</sub>(OTerpy)] (L<sup>1</sup>). N<sub>3</sub>P<sub>3</sub>(OPh)<sub>5</sub>Cl (100 mg, 0.16 mmol) was added to a solution containing HOTerpy (40 mg, 0.16 mmol) and NaH (9 mg, 0.22 mmol) in THF (30 mL). After stirring at reflux for 3 days, the solvent was removed under reduced pressure, leaving a white oil, which was washed with CH<sub>2</sub>Cl<sub>2</sub>/water and dried over MgSO<sub>4</sub>. The oil was purified by column chromatography on silica gel with CH<sub>2</sub>Cl<sub>2</sub>/hexane (1:1) as the eluent, producing a colorless viscous oil. Yield: 73 mg (54%). ESMS: *m/z* 849 ([N<sub>3</sub>P<sub>3</sub>(OPh)<sub>5</sub>(OTerpy)H]<sup>+</sup>). <sup>31</sup>P{<sup>1</sup>H} NMR (CDCl<sub>3</sub>): δ 8.9 (s, 3P). <sup>1</sup>H NMR (CDCl<sub>3</sub>): δ 8.68 (d (s), 2H), 8.62 (d (s), 2H), 8.38 (s, 2H), 7.85 (t (s), 2H), 7.32 (t (s), 2H), 7.28 (t (s), 2H), 7.20 (d (s), 10H), 7.16 (t (s), 8H), 7.05 (d (s), 5 H). Anal. Calcd for C<sub>45</sub>H<sub>36</sub>N<sub>6</sub>O<sub>6</sub>P<sub>3</sub>·CH<sub>2</sub>Cl<sub>2</sub>·2C<sub>6</sub>H<sub>14</sub>: C, 63.30; H, 6.17; N, 7.49. Found: C, 63.34; H, 5.95; N, 7.30.

[N<sub>3</sub>P<sub>3</sub>(OPh)<sub>5</sub>(OPhTerpy)] (L<sup>2</sup>). N<sub>3</sub>P<sub>3</sub>(OPh)<sub>5</sub>Cl (100 mg, 0.16 mmol) was added to a solution containing HOPhTerpy·3HCl (75 mg, 0.17 mmol) and NaH (34 mg, 0.85 mmol) in THF (30 mL). After stirring at reflux overnight, the solvent was removed under reduced pressure, leaving a white oil, which was washed with CH<sub>2</sub>Cl<sub>2</sub>/water and dried over MgSO<sub>4</sub>. The oil was purified by column chromatography on silica gel with CH<sub>2</sub>Cl<sub>2</sub>:hexane (1:1) as the eluent, producing a colorless viscous oil. Yield: 130 mg (88%). ESMS: *m/z* 926 ([N<sub>3</sub>P<sub>3</sub>(OPh)<sub>5</sub>(OPhTerpy)H]<sup>+</sup>). <sup>31</sup>P{<sup>1</sup>H} NMR (CDCl<sub>3</sub>): δ 9.50. <sup>1</sup>H NMR (CDCl<sub>3</sub>): δ 8.76 (d (s), 2H), 8.72 (s, 2H), 8.70 (d (s), 2H), 7.89 (t (s), 2H), 7.69 (d (s), 2H), 7.36 (t (s), 2H), 7.27–7.20 (m, 10H), 7.17–7.16 (m, 5H), 7.08 (d (s), 2H), 7.04–6.97 (m, 10H). Anal. Calcd for C<sub>51</sub>H<sub>39</sub>N<sub>6</sub>O<sub>6</sub>P<sub>3</sub>·0.66C<sub>6</sub>H<sub>14</sub>: C, 67.25; H, 4.96; N, 8.56. Found: C, 67.16; H, 4.98; N, 8.23.

{[NP(OPh<sup>tBu</sup>)(OTerpy)]<sub>0.20</sub>[NP(OPh<sup>tBu</sup>)<sub>2</sub>]<sub>0.60</sub>[NP(OPh<sup>tBu</sup>)Cl]<sub>0.20</sub>]<sub>*n*</sub> (L<sup>1P</sup>). {NPCL<sub>2</sub>]<sub>*n*</sub> (1 g, 8.77 mmol) was dissolved in THF (50 mL); to this was added a solution containing HOPh<sup>tBu</sup> (526 mg, 3.51 mmol), HOTerpy

(436 mg, 1.76 mmol), and NaH (158 mg, 3.95 mmol) in THF (30 mL). The solution was refluxed for 2 h before an additional solution of HOPh<sup>tBu</sup> (526 mg, 3.51 mmol), NaH (140 mg, 3.51 mmol), and TBAB (10 mol %) in THF (30 mL) was added. This solution was refluxed overnight before an additional solution of HOPh<sup>tBu</sup> (2.63 g, 17.54 mmol) in THF (30 mL) and toluene (30 mL) was added. This solution was refluxed for an additional 2 days. The solvent was removed on a rotary evaporator. The solid was redissolved in a minimal amount of THF; this viscous oil was slowly poured into slightly acidic water, forming thin white strings. The white strings of polymer were collected, dissolved in CH<sub>2</sub>Cl<sub>2</sub>, and then reduced in volume to form the viscous oil again; this was slowly poured into methanol, forming white strings of polymer. This process was repeated one more time before drying under a high vacuum. Yield: 1.20 g (40%). <sup>31</sup>P{<sup>1</sup>H} NMR (CDCl<sub>3</sub>): δ -15.38 (1P), -18.43 (4P). <sup>1</sup>H NMR (CDCl<sub>3</sub>): δ 8.52 (4H), 7.76 (2H), 6.99 (66H), 1.16 (72H). Anal. Calcd for C<sub>95</sub>H<sub>114</sub>N<sub>8</sub>O<sub>6</sub>P<sub>3</sub>Cl·1.33NaCl: C, 64.10; H, 6.45; N, 6.29; Cl, 4.65. Found: C, 64.24; H, 6.57; N, 6.40; Cl, 4.63. *M<sub>w</sub>*: 399000 (PDI = 2.97). *T<sub>g</sub>*: 39 °C.

{[NP(OPh<sup>tBu</sup>)(OPhTerpy)]<sub>0.20</sub>[NP(OPh<sup>tBu</sup>)<sub>2</sub>]<sub>0.74</sub>[NP(OPh<sup>tBu</sup>)Cl]<sub>0.06</sub>]<sub>*n*</sub> (L<sup>2P</sup>). {NPCL<sub>2</sub>]<sub>*n*</sub> (1 g, 8.77 mmol) was dissolved in THF (50 mL); to this was added a solution containing HOPh<sup>tBu</sup> (526 mg, 3.51 mmol), HOPhTerpy (572 mg, 1.76 mmol), and NaH (158 mg, 3.95 mmol) in THF (30 mL). The solution was refluxed for 2 h before an additional solution of HOPh<sup>tBu</sup> (526 mg, 3.51 mmol), NaH (140 mg, 3.51 mmol), and TBAB (10 mol %) in THF (30 mL) was added. This solution was refluxed overnight before an additional solution of HOPh<sup>tBu</sup> (2.63 g, 17.54 mmol) in THF (30 mL) and toluene (30 mL) was added. This solution was refluxed for an additional 2 days. The solvent was removed on a rotary evaporator. The solid was redissolved in a minimal amount of THF; this viscous oil was slowly poured into slightly acidic water, forming thin white strings. The white strings of polymer were collected, dissolved in CH<sub>2</sub>Cl<sub>2</sub>, and then reduced in volume to form the viscous oil again; this was slowly poured into methanol, forming white strings of polymer. This process was repeated one more time before drying under a high vacuum. Yield: 1.60 g (50%) <sup>31</sup>P{<sup>1</sup>H} NMR (CDCl<sub>3</sub>): δ -15.38 (0.3P), -18.58 (4.7P). <sup>1</sup>H NMR (CDCl<sub>3</sub>): δ 8.67 (4H), 7.87 (2H), 7.33 (2H), 6.98 (40.8), 1.12 (78.3). Anal. Calcd for C<sub>108</sub>H<sub>127.1</sub>N<sub>8</sub>O<sub>9.7</sub>P<sub>5</sub>Cl<sub>0.3</sub>·1.33NaCl: C, 67.00; H, 6.62; N, 5.79; Cl, 2.99. Found: C, 63.44; H, 7.06; N, 4.89; Cl, 3.06. *M<sub>w</sub>*: 795000 (PDI = 2.01). *T<sub>g</sub>*: 39 °C.

[Fe(L<sup>1</sup>)<sub>2</sub>](ClO<sub>4</sub>)<sub>2</sub> (1a). To a stirred solution of L<sup>1</sup> (100 mg, 0.11 mmol) in MeOH/CHCl<sub>3</sub> (1:1, 8 mL) was added Fe(ClO<sub>4</sub>)<sub>2</sub>·6H<sub>2</sub>O (4.0 mg, 0.066 mmol), immediately turning the solution purple. Stirring was continued for 30 min before the solvent was removed under reduced pressure. The solid was dissolved in CHCl<sub>3</sub> and filtered through Celite. The filtrate was dried under reduced pressure, leaving a purple solid. Crystals were grown by dissolving the solid in acetonitrile and diffusing in diethyl ether, producing thin needles. Yield: 78 mg (68%). ESMS: *m/z* 876 ([Fe(L<sup>1</sup>)<sub>2</sub>]<sup>2+</sup>). <sup>31</sup>P{<sup>1</sup>H} NMR (CD<sub>3</sub>CN): δ 11.1 (m, 6P). <sup>1</sup>H NMR (CD<sub>3</sub>CN): δ 8.70 (s, 4H), 8.18 (d (s), 4H), 7.68 (t (s), 4H), 7.42 (t (s), 4H), 7.36–7.15 (m, 42H), 7.04 (t (s), 4H), 6.98 (d (s), 4H), 6.93 (d (s), 4H). Anal. Calcd for C<sub>90</sub>H<sub>70</sub>Cl<sub>2</sub>FeN<sub>12</sub>O<sub>26</sub>P<sub>6</sub>·2.5C<sub>4</sub>H<sub>10</sub>O·2H<sub>2</sub>O: C, 55.16; H, 4.77; N, 7.72. Found: C, 55.31; H, 4.60; N, 7.68.

[Fe(L<sup>1</sup>)<sub>2</sub>](PF<sub>6</sub>)<sub>2</sub> (1b). To a stirred solution of L<sup>1</sup> (100 mg, 0.11 mmol) in MeOH/CHCl<sub>3</sub> (1:1, 8 mL) was added FeCl<sub>2</sub>·4H<sub>2</sub>O (22 mg, 0.11 mmol), immediately turning the solution purple. Stirring was continued for 30 min before the solvent was removed under reduced pressure, leaving a purple solid. The solid was dissolved in CHCl<sub>3</sub> and filtered through Celite. The filtrate was dried under reduced pressure, leaving a purple solid. This solid was dissolved in CH<sub>3</sub>CN (5 mL), and Ag(CH<sub>3</sub>CN)<sub>4</sub>(PF<sub>6</sub>) (85 mg, 0.33 mmol) was added, with a white precipitate immediately forming. The solution was stirred for 30 min before the solvent was removed under reduced pressure. The solid was dissolved in CHCl<sub>3</sub> and filtered through Celite. The filtrate was dried under reduced pressure, leaving a purple solid. The purple solid was dissolved in CHCl<sub>3</sub> and precipitated with hexane for analysis. Crystals were grown by dissolving in CH<sub>3</sub>CN and vapor-diffusing with diethyl ether, producing thin needles. Yield: 76 mg (64%). ESMS: *m/z* 876

Table 1. Crystal and Refinement Data for 1a·CH<sub>3</sub>CN, 1b·CH<sub>3</sub>CN, and 2b

	1a·CH <sub>3</sub> CN	1b·CH <sub>3</sub> CN	2b
molecular formula	C <sub>92</sub> H <sub>73</sub> Cl <sub>2</sub> FeN <sub>13</sub> O <sub>20</sub> P <sub>6</sub>	C <sub>92</sub> H <sub>73</sub> F <sub>12</sub> FeN <sub>13</sub> O <sub>12</sub> P <sub>8</sub>	C <sub>102</sub> H <sub>78</sub> F <sub>12</sub> FeN <sub>12</sub> O <sub>12</sub> P <sub>8</sub>
<i>M</i> (g mol <sup>-1</sup> )	1993.23	2084.26	2195.40
<i>T</i> (K)	123(2)	90(2)	90(2)
cryst syst	triclinic	triclinic	triclinic
space group	<i>P</i> <sub>1</sub>	<i>P</i> <sub>1</sub>	<i>P</i> <sub>1</sub>
<i>a</i> (Å)	14.767(3)	15.042(8)	9.823(3)
<i>b</i> (Å)	16.334(3)	16.340(10)	20.681(9)
<i>c</i> (Å)	21.024(4)	20.999(13)	24.932(10)
$\alpha$ (deg)	104.25(3)	100.59(5)	86.15(3)
$\beta$ (deg)	100.82(3)	91.53(3)	84.188(14)
$\gamma$ (deg)	91.04(3)	91.53(5)	87.457(13)
<i>V</i> (Å <sup>3</sup> )	4816.7(17)	4936(5)	5024(3)
<i>Z</i>	2	2	2
$\mu$ (Mo <i>K</i> $\alpha$ ) (mm <sup>-1</sup> )		0.368	0.368
$\mu$ (Cu <i>K</i> $\alpha$ ) (mm <sup>-1</sup> )	3.317		
$\rho_{\text{calc}}$ (g cm <sup>-3</sup> )	1.374	1.402	1.451
$2\theta_{\text{max}}$ (deg)	133.16	58.28	56.56
no. of unique reflns	15495	26163	24825
data/restraints/param	15495/96/1208	26163/130/1264	24825/297/1359
final <i>R</i> indices [ <i>I</i> > 2 $\sigma$ ( <i>I</i> )]	<i>R</i> 1 = 0.0727, <i>wR</i> 2 = 0.1879	<i>R</i> 1 = 0.0585, <i>wR</i> 2 = 0.1320	<i>R</i> 1 = 0.0710, <i>wR</i> 2 = 0.1843
<i>R</i> indices (all data)	<i>R</i> 1 = 0.0955, <i>wR</i> 2 = 0.2111	<i>R</i> 1 = 0.0748, <i>wR</i> 2 = 0.1385	<i>R</i> 1 = 0.1120, <i>wR</i> 2 = 0.2069
GOF on <i>F</i> <sup>2</sup>	1.088	1.084	0.926

([Fe(L<sup>1</sup>)<sub>2</sub>]<sup>2+</sup>). <sup>31</sup>P{<sup>1</sup>H} NMR (CD<sub>3</sub>CN):  $\delta$  10.6 (m, 6P), -143.1 (sep (792), 2P). <sup>1</sup>H NMR (CD<sub>3</sub>CN):  $\delta$  8.70 (s, 4H), 8.17 (d (8), 4H), 7.78 (t (8), 4H), 7.39 (t (8), 4H), 7.32–7.12 (m, 42 H), 7.04 (t (8), 4H), 7.02 (d (6), 4H), 6.93 (d (8), 4H). Anal. Calcd for C<sub>90</sub>H<sub>70</sub>F<sub>12</sub>FeN<sub>12</sub>O<sub>12</sub>P<sub>8</sub>·3CHCl<sub>3</sub>: C, 46.52; H, 3.06; N, 7.00. Found: C, 46.09; H, 3.09; N, 6.96.

[Fe(L<sup>2</sup>)<sub>2</sub>](ClO<sub>4</sub>)<sub>2</sub> (**2a**). The same procedure as that for **1a** was used; however, L<sup>2</sup> was used in place of L<sup>1</sup>, forming a purple solid. Nondiffractable purple crystals were formed by vapor-diffusing diethyl ether into acetonitrile. The solid was dissolved in chloroform and precipitated with hexane for analysis. Yield: 60 mg (53%). ESMS: *m/z* 953 ([Fe(L<sup>2</sup>)<sub>2</sub>]<sup>2+</sup>). <sup>31</sup>P{<sup>1</sup>H} NMR (CD<sub>3</sub>CN):  $\delta$  10.3 (s, 6P). <sup>1</sup>H NMR (CD<sub>3</sub>CN):  $\delta$  9.14 (s, 4H), 8.65 (d (8), 4H), 8.25 (d (8), 4H), 7.59 (t (8), 4H), 7.42–7.29 (m, 26H), 7.24 (d (8), 4H), 7.13 (t (8), 12H), 7.04 (d (8), 4H), 6.98 (d (8), 8H). Anal. Calcd for C<sub>102</sub>H<sub>78</sub>Cl<sub>2</sub>FeN<sub>12</sub>O<sub>20</sub>P<sub>8</sub>·0.5CHCl<sub>3</sub>: C, 56.89; H, 3.66; N, 7.77. Found: C, 56.76; H, 3.41; N, 7.76.

[Fe(L<sup>2</sup>)<sub>2</sub>](PF<sub>6</sub>)<sub>2</sub> (**2b**). The same procedure as that for **1b** was used; however, L<sup>2</sup> was used in place of L<sup>1</sup>. The purple solid was dissolved in CHCl<sub>3</sub> and precipitated with hexane for analysis. Purple crystals were grown via vapor diffusion of Et<sub>2</sub>O into a CH<sub>3</sub>CN solution. Yield: 72 mg (59%). ESMS: *m/z* 953 ([Fe(L<sup>2</sup>)<sub>2</sub>]<sup>2+</sup>). <sup>31</sup>P{<sup>1</sup>H} NMR (CD<sub>3</sub>CN):  $\delta$  10.3 (s, 6P), -143.2 (sep (708), 2P). <sup>1</sup>H NMR (CD<sub>3</sub>CN):  $\delta$  9.14 (s, 4H), 8.65 (d (8), 4H), 8.25 (d (8), 4H), 7.59 (t (8), 4H), 7.42–7.29 (m, 26H), 7.24 (d (8), 4H), 7.13 (t (8), 12H), 7.04 (d (8), 4H), 6.98 (d (8), 8H). Anal. Calcd for C<sub>102</sub>H<sub>78</sub>F<sub>12</sub>FeN<sub>12</sub>O<sub>12</sub>P<sub>8</sub>·1.5CHCl<sub>3</sub>: C, 52.33; H, 3.37; N, 7.07. Found: C, 52.26; H, 3.63; N, 7.18.

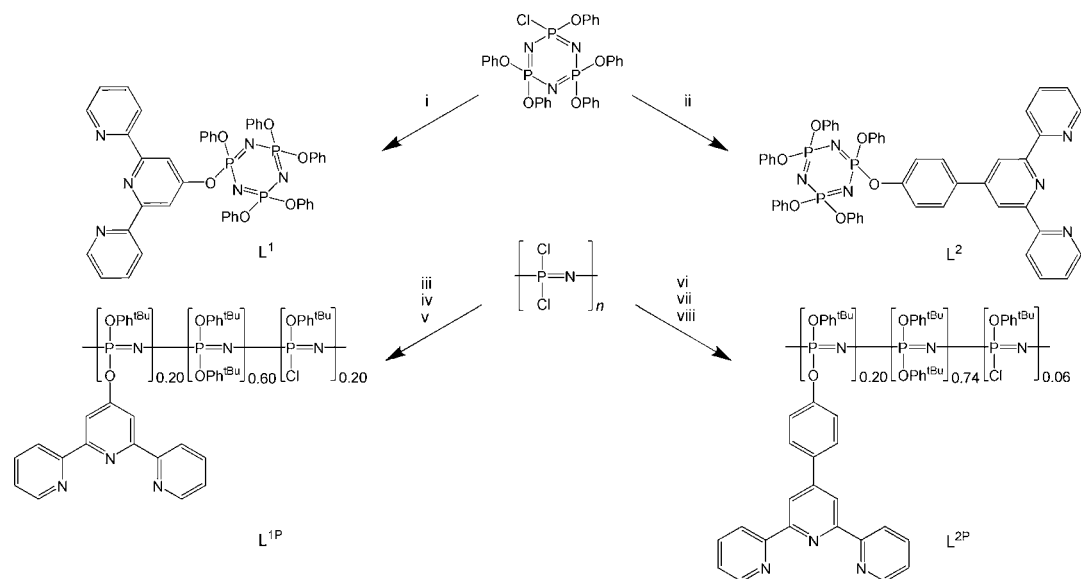
[Fe(L<sup>1P</sup>)<sub>2</sub>](ClO<sub>4</sub>)<sub>2</sub> (**3a**). L<sup>1P</sup> (300 mg, 0.17 mmol) was dissolved in CHCl<sub>3</sub> (50 mL); once dissolved, CH<sub>3</sub>CN (0.5 mL) was added. Fe(ClO<sub>4</sub>)<sub>2</sub>·6H<sub>2</sub>O (32 mg, 0.088 mmol) was added to the solution, forming a purple solution over 1 h. All characterisations in the solution phase were recorded using this solution. The volume of the solvent was reduced to 25 mL under a vacuum; methanol was gradually added until a precipitate formed. The supernatant liquid was decanted before additional methanol was added, the solution was sonicated, and then the supernatant liquid was decanted again. The remaining solid was dried under a vacuum, producing a purple solid. Yield: 138 mg (42%). <sup>31</sup>P{<sup>1</sup>H} NMR:  $\delta$  -14.95 (2P), -18.20 (8P). Anal. Calcd for C<sub>190</sub>H<sub>228</sub>Cl<sub>4</sub>FeN<sub>16</sub>O<sub>26</sub>P<sub>10</sub>·0.5CHCl<sub>3</sub>: C, 61.52; H, 6.19; N, 6.03; Cl, 5.24. Found: C, 57.63; H, 6.44; N, 6.13; Cl, 5.28. *T*<sub>g</sub>: not visible.

[Fe(L<sup>2P</sup>)<sub>2</sub>](ClO<sub>4</sub>)<sub>2</sub> (**4a**). The same method as that for **3a** was used except L<sup>2P</sup> was used in place of L<sup>1P</sup>, forming a purple solid. Yield: 172 mg (54%). <sup>31</sup>P{<sup>1</sup>H} NMR:  $\delta$  -14.95 (0.6P), -18.20 (9.4P). Anal. Calcd for C<sub>216</sub>H<sub>252.9</sub>Cl<sub>2.6</sub>FeN<sub>16</sub>O<sub>27.4</sub>P<sub>10</sub>·2.75CHCl<sub>3</sub>: C, 61.13; H, 6.00; N, 5.21; Cl, 8.95. Found: C, 58.07; H, 6.26; N, 5.74; Cl, 9.22. *T*<sub>g</sub>: 44 °C.

**X-ray Crystallography.** The X-ray data for **1b**·CH<sub>3</sub>CN and **2b** was collected on a Siemens P4 four-circle diffractometer, using a Siemens SMART 1K charge-coupled detector (CCD) area detector. The crystal was mounted in an inert oil, transferred into the cold gas stream of the detector, and irradiated with graphite-monochromated Mo *K* $\alpha$  ( $\lambda$  = 0.71073 Å) X-rays. The data were collected by the SMART program and processed with SAINT to apply Lorentz and polarization corrections to diffract spots (integrated three-dimensionally). **1a**·CH<sub>3</sub>CN data were collected at low temperature with a Rigaku-Spider X-ray diffractometer, comprising a Rigaku MM007 microfocus copper rotating-anode generator, high-flux Osmic monochromating and focusing multilayer mirror optics (Cu *K* radiation,  $\lambda$  = 1.5418 Å), and a curved image-plate detector. CrystalClear was utilized for data collection and *FSProcess* in *PROCESS-AUTO* for cell refinement and data reduction. Crystal refinement data are given in Table 1. The structures were solved by direct methods and refined using both the *SHELXTL*<sup>30</sup> and *OLEX*<sup>2,31</sup> programs. Hydrogen atoms were located at ideal positions.

For the solution of **1a**·CH<sub>3</sub>CN, the electron density (58 e cell<sup>-1</sup>) of the occupationally and positionally disordered diethyl ether molecules was removed by using *PLATON/SQUEEZE*<sup>32</sup> and 489.1 Å<sup>3</sup> was left accessible by the void. A similar treatment was used for the solvent molecules in **1b**·CH<sub>3</sub>CN, for which 63 e cell<sup>-1</sup> was removed and 455.0 Å<sup>3</sup> was accessible by the void, and **2b**, for which 57 e cell<sup>-1</sup> was removed and 315.5 Å<sup>3</sup> was accessible by the void.

**Instrumentation.** Microanalyses were performed by Campbell Microanalytical Laboratory, University of Otago, Otago, New Zealand, and assigned using CHN. <sup>31</sup>P{<sup>1</sup>H} NMR was performed on a Bruker Avance 400 spectrometer and <sup>1</sup>H NMR on a Bruker Avance 500 spectrometer. Electrospray ionization mass spectrometry (ESI-MS) spectra were obtained from acetonitrile solutions on a Micromass ZMD spectrometer run in the positive-ion mode. Listed peaks correspond to the most abundant isotopomer; assignments were made by a comparison of the observed and simulated spectra. All ground-state vibrational measurements were taken using KBr disks on a

Scheme 1. Schemes for the Synthesis of Ligands  $L^1$ ,  $L^2$ ,  $L^{1P}$ , and  $L^{2P}$ <sup>a</sup>

<sup>a</sup>(i) NaH, HOTerpy; (ii) NaH, HOPhTerpy; (iii) 10% HOPh<sup>tBu</sup>, NaH; (iv) HOTerpy, TBAB; (v) HOPh<sup>tBu</sup>, NaH; (vi) 10% HOPh<sup>tBu</sup>, NaH; (vii) HOPhTerpy, TBAB; (viii) HOPh<sup>tBu</sup>, NaH.

Nicolet 5700 Fourier transform infrared (FT-IR) spectrometer. Continuous-wave excitation was used for all Raman measurements. UV–visible absorbance spectra were recorded on an Oceans Optics USB2000+ UV–visible spectrophotometer in acetonitrile for complexes **1a**, **1b**, **2a**, and **2b** at  $10^{-5}$  M and in chloroform for **3a** and **4a** at  $10^{-5}$  M. Cyclic voltammetry was obtained using a glassy carbon working electrode, a platinum counter electrode, and an Ag/AgCl reference electrode;  $\nu = 0.1$  V s<sup>-1</sup> recorded in acetonitrile, 0.1 M TBAClO<sub>4</sub> at  $10^{-3}$  M for complexes **1a** and **2a**, and 0.1 M TBAPF<sub>6</sub> at  $10^{-3}$  M for complexes **1b** and **2b**. Differential scanning calorimetry (DSC) measurements were performed on a Perkin-Elmer DSC-7 unit controlled by a PE7500 computer at The Pennsylvania State University, University Park, PA. Each sample was annealed twice, from 22 to 80 °C and from -100 to +100 °C, and then from -100 to +150 °C.

Resonance Raman measurements were carried out based on a modified version of a system described previously.<sup>34–36</sup> Spectra of solid-state samples at 79, 298, and 362 K were acquired with a number of excitation wavelengths. Temperature control was achieved by utilizing a variable-temperature cell (Specac, Woodstock, GA) and a high-stability temperature controller (Specac, Woodstock, GA). Vacuum purging of the cell was used to minimize condensation and frosting of the quartz window of the variable-temperature cell. For excitation at 350.7 and 568.1 nm, a continuous-wave Innova I-302 krypton-ion laser (Coherent, Inc., Santa, CA) was used. For excitation at 457.9 and 514.5 nm, an Innova Sabre DBW argon-ion laser (Coherent, Inc., Santa, CA) was used. The beam was passed through either a Pellin-Broca prism (for 350.7, 457.9, and 514.5 nm) or a holographic laser bandpass filter (Kaiser Optical Systems, Inc., Ann Arbor, MI) and subsequently two irises in order to remove unwanted laser lines. The beam power was adjusted between 20 and 40 mW at the sample, depending on the wavelength used. The sample and collection lens were arranged in a 180° backscattering geometry, where the collection lens also served to focus the excitation beam on the sample. The Raman photons were focused on the entrance slit of an Acton Research SpectraPro500i spectrograph (Princeton Instruments, Inc., Trenton, NJ) with a 1200 grooves mm<sup>-1</sup> grating. The slit width was set to 50  $\mu$ m, giving a resolution of ca. 2 cm<sup>-1</sup>. Radiation from Raleigh and Mie scattering was attenuated using a notch filter (Kaiser Optical Systems, Inc., Ann Arbor, MI) for 568.1 nm and RazorEdge filters (Semrock, Inc., Rochester, NY) for other wavelengths. The dispersed photons were detected using a Princeton Instruments liquid-nitrogen-cooled 1152-EUV CCD controlled by a Princeton Instru-

ments ST-130 controller. WinSpec/32 software (Roper Scientific, Inc., Trenton, NJ) was used to control the CCD, and spectra were analyzed using GRAMS/32 (Galactic Industries Corp., Salem, NH) software. Wavelength calibration was achieved using a reference sample made from 1:1 toluene/acetonitrile, and general alignment was done using a solid sample of carbamazepine.

<sup>57</sup>Fe Mössbauer spectra were recorded at the University of Otago. Approximately 30 mg of sample was placed in a nylon sample holder (12.8 mm diameter, 1.6 mm thickness) with Kapton windows. Mössbauer spectra were measured on a Mössbauer spectrometer from SEE Co. (Science Engineering & Education Co., Edina, MN) equipped with a closed-cycle refrigerator system from Janis Research Co. and Sumitomo Heavy Industries Ltd. Data were collected in constant acceleration mode in transmission geometry with an applied field of 47 mT parallel to the  $\gamma$ -rays. The zero velocity of the Mössbauer spectra refers to the centroid of the room temperature spectrum of a 25  $\mu$ m metallic iron foil. Analysis of the spectra was conducted using the WMOSS program (SEE Co., formerly WEB Research Co., Edina, MN).

Magnetic susceptibilities were determined using a Quantum Design Inc. SQUID MPMS5 magnetometer with the ~25 mg samples held in a calibrated gel capsule that was placed in the center of a drinking straw that was fixed to the end of the sample rod. A direct-current field of 1 T was used. The instrument was calibrated against a palladium pellet of accurately known susceptibility provided by Quantum Design Inc. and checked against the temperature-dependent (TD) behavior of CuSO<sub>4</sub>·5H<sub>2</sub>O.

**Computational Details.** DFT calculations were carried out using the *Gaussian09* package (Gaussian, Inc.).<sup>37</sup> Frequency-dependent and TD calculations were performed on optimized ground-state structures; all results are displayed using *GaussView*.<sup>38</sup> All calculations used the 6-31G(d) basis set, employing two different levels, OLYP and B3LYP. The vibrational spectra generated by both levels were compared to the measured vibrational data, determining OLYP to be the most accurate level. An unambiguous assignment of the vibrational modes from a visual comparison of the spectra was possible for most peaks. TD-DFT calculations were carried out in an acetonitrile solvent field using the self-consistent reaction field polarizable continuum model method, which creates the solvent cavity via a set of overlapping spheres. Geometry optimizations were not carried out in a solvent field because these are difficult to achieve for molecules of this size; however, the correlation is found to be better than that for calculations where solvent contributions have been completely neglected.

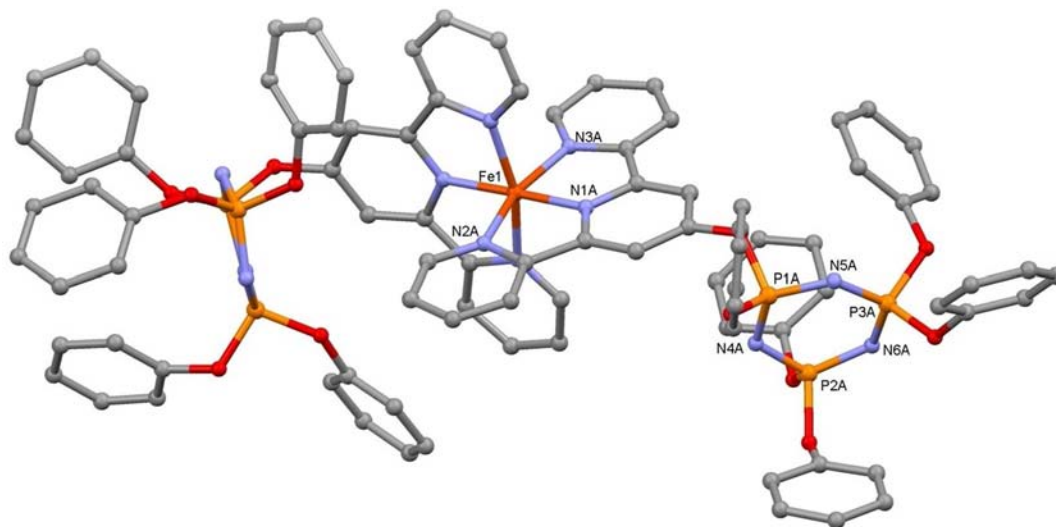


Figure 1. Crystal structure of **1a**·CH<sub>3</sub>CN or **1b**·CH<sub>3</sub>CN. Hydrogen atoms, solvents, and anions are removed for clarity.

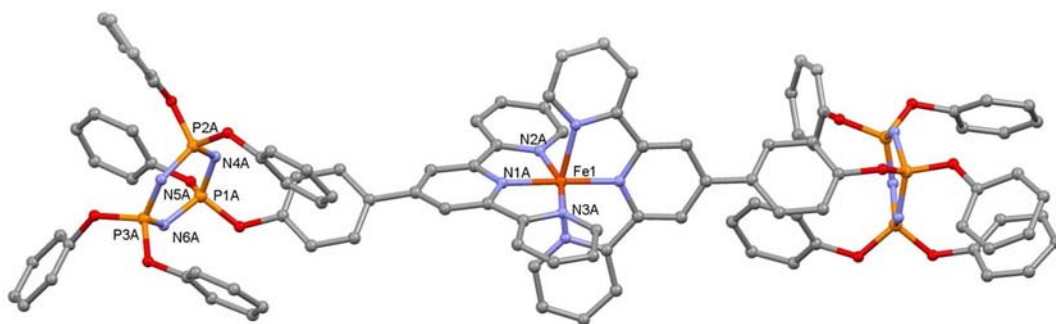


Figure 2. Crystal structure of **2b**. Hydrogen atoms, solvents, and anions are removed for clarity.

The two different levels for computational models (B3LYP and OLYP) with a 6-31G(d) basis set were compared to vibrational data collected to determine which was the most accurate in addition to validating the models. Higher-level basis sets were not explored because of the size of the molecule, making such calculations unfeasible. The B3LYP frequencies were scaled by 0.9613<sup>39</sup> and OLYP by 0.9782.<sup>40</sup> The assignments of the spectra were made using each level and the MAD values determined for all of the assigned peaks (Table S2.1 in the Supporting Information). These values indicated that there was little difference between the levels, but a comparison between the measured and calculated bond lengths indicated that the OLYP models were 1 order of magnitude more accurate than the B3LYP models (Table S2.2–3 in the Supporting Information).

## RESULTS AND DISCUSSION

**Synthesis.** Each of the CTP ligands was synthesized by reacting the sodium salt of each of the substituents (HOPhTeryp or HOTeryp) with N<sub>3</sub>P<sub>3</sub>(OPh)<sub>5</sub>Cl (see Scheme 1). In the case of L<sup>2</sup>, the reaction was rapid, requiring only 12 h; however, L<sup>1</sup> required 3 days. Such a difference in the reaction time was likely due to stabilization of the eneone tautomer for HOTeryp,<sup>41</sup> making it less reactive than the phenol tautomer of HOPhTeryp. The <sup>31</sup>P NMR spectra of both L<sup>1</sup> and L<sup>2</sup> display pseudo singlet signals; it is proposed that this occurs because OPh, OTeryp, and OPhTeryp groups have such similar electronegativities that, with the resolution of the instrument, each of the phosphorus atoms are in an identical environment.

The different reaction rate observed in the CTP ligands was reflected in the synthesis of the polymers, with HOTeryp (L<sup>1P</sup>)

taking 2 days to react with the chloropolymer and HOPhTeryp (L<sup>2P</sup>) only requiring 12 h. L<sup>1P</sup> has a lower molecular weight than L<sup>2P</sup> possibly because of the increased reaction time or maybe the substituent decay described by Kirk.<sup>9</sup> An additional feature that is observed in the polymer synthesis is the large number of unsubstituted chlorines. Allcock suggested that this behavior occurs because the bulky *tert*-butyl groups cause steric hindrance, preventing further reaction.<sup>29</sup> In the case of L<sup>1P</sup>, the OTeryp groups are held close to the polymer backbone, causing additional steric hindrance and preventing further substitution of the chlorines, as determined by the combination of elemental analysis and <sup>31</sup>P NMR spectroscopy. Variations of base, promoters, and solvents were tried; however, none of these significantly improved the reaction's completeness. The difficulties associated with the process are consistent with reports in the literature.<sup>29</sup> Trifluoroethoxy was not selected as a pendant group because Ainscough et al.<sup>12</sup> previously demonstrated that it has a tendency to displace aromatic substituents. Despite the residual P–Cl units, the polymers remained soluble to aqueous workup and remained stable for several months.

The CTP iron(II) complex formation was similar to that of analogues using unsubstituted ligands. A total of 2 equiv of the ligands was rapidly reacted with the respective iron(II) salts in solution, forming the unit of [Fe(L)<sub>2</sub>]<sub>2</sub> (**1a**, **1b**, **2a**, and **2b**). In the case of the polymers, it is suspected that, because of iron(II) high reactivity, intrapolymer loops were formed. Such behavior is suspected because the polymer remains soluble for

up to 1 week. However, if the solution was left to stand for over 1 week or if it was precipitated, the resulting purple solids could not be dissolved in any solvents at any temperature. This behavior suggests that the polymer has formed an interpolymer cross-linked network. Only small differences were observed in the  $T_g$  values between the polymer ligands and the corresponding iron complexes. However, Carriedo et al. demonstrated that gold phosphine cross-linked polymers with low levels of cross-linking do not show large increases in the  $T_g$  values.<sup>18</sup>

**Molecular Structures.** The crystal structures of complexes **1a**·CH<sub>3</sub>CN (Figure 1), **1b**·CH<sub>3</sub>CN (Figure 1), and **2b** (Figure 2) show the expected coordination mode with iron(II), with the coordination sphere being comprised of a “FeN<sub>6</sub>” donor set. Selected bond lengths and angles are given in the Supporting Information (Table S1.1–6). The axial Terpy–iron bonds of both **1a** and **1b** are Fe1–N1A and Fe1–N1B = 1.886(2) and 1.889(2) Å, respectively, and Fe1–N1A and Fe1–N1B = 1.883(3) and 1.882(4) Å, respectively, for **2b**. In addition, both **1a**·CH<sub>3</sub>CN and **1b**·CH<sub>3</sub>CN form isomorphous structures with the anions in identical positions, with two of the nongeminal pendant phenoxy groups displaying  $\pi$ –H interactions with the Terpy units. However, this is not observed for **2b**; because of inclusion of a phenyl spacer, the phenoxy groups are too far away from the Terpy unit to be involved in  $\pi$ –H interactions. The axial bond lengths of **2b** are 1.886(3) (Fe1–N1A) and 1.878(3) Å (Fe1–N1B), similar to those of **1a**·CH<sub>3</sub>CN and **1b**·CH<sub>3</sub>CN. The Fe–N bond lengths for **1a**·MeCN, **1b**·MeCN, and **2b** are all typical of low-spin iron(II) existing at these temperatures (123 and 90 K). Because the anions are shown to sit in the same position for each complex, it can be assumed that the anions behave in the same fashion when in the polymer.

**Electrochemistry.** Each of the CTP complexes displayed reductions associated with ligands and a reversible metal-based oxidation (Fe<sup>II</sup>/Fe<sup>III</sup>) with an  $E_{1/2}$  of 0.854 V for **1a** and **1b** and 0.940 V for **2a** and **2b** (see Table 2). Compared to the

**Table 2. Electrochemical Data for Compounds 1a, 1b, 2a, and 2b**

complex	$E_{1/2ox}$ (V)	$E_{1/2red}$ (V)	$E_{1/2red}$ (V)
<b>1a</b>	0.854 (65)	–1.234 (irr)	
<b>1b</b>	0.854 (68)	–1.237 (irr)	
<b>2a</b>	0.940 (83)	–1.259 (73)	–1.514 (irr)
<b>2b</b>	0.940 (83)	–1.259 (73)	–1.514 (irr)

unsubstituted analogues ([Fe(Terpy)<sub>2</sub>](PF<sub>6</sub>)<sub>2</sub> ( $E_{1/2ox}$  = 0.770 V)<sup>42</sup> and [Fe(PhTerpy)<sub>2</sub>](ClO<sub>4</sub>)<sub>2</sub> ( $E_{1/2ox}$  = 1.105 V)<sup>43,44</sup> respectively), the oxidation potentials of **1a** and **1b** show a cathodic shift due to the electron-withdrawing effects of the phosphazene ether group. However, **2a** and **2b** have an anodic shift due to the phenyl spacer acting as an electron-donating group and isolating the FeTerpy unit from the effects of the phosphazene ether group. Electrochemical data for the PP complexes (**3a** and **4a**) could not be obtained because of the low conductivity of the solution.

**Electronic Spectroscopy.** The electronic spectra of complexes **1a**, **1b**, **2a**, **2b**, **3a**, and **4a** are shown in Figure 3. The first 10 calculated transitions with nonzero oscillator strengths can be found in the Supporting Information (Tables S3.1 and S3.2). The absorption spectra of complexes with ClO<sub>4</sub><sup>–</sup> and PF<sub>6</sub><sup>–</sup> anions are near-identical, indicating little or no

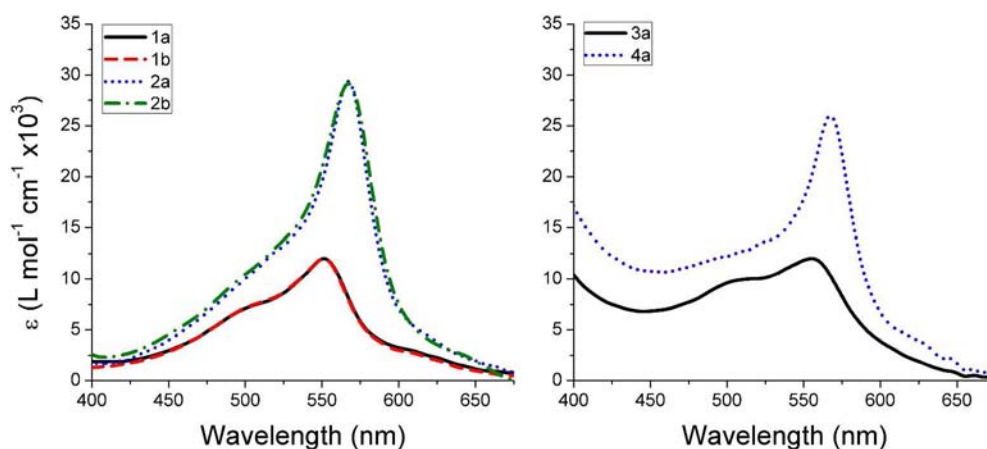
interaction with the anion in the solution phase. The lowest-energy peaks have been attributed to metal-to-ligand charge-transfer (MLCT) transitions, which are summarized in Table 3. Furthermore, shoulders are observed to the red of the MLCT band, at ca. 625 nm for all complexes, which are consistent with iron-centered d–d transitions found in related systems. For complexes **1a**, **1b**, **2a**, and **2b**, these transitions are near-identical with their phosphazene-free analogues, [Fe(Terpy)<sub>2</sub>](ClO<sub>4</sub>)<sub>2</sub><sup>45</sup> and [Fe(PhTerpy)<sub>2</sub>](ClO<sub>4</sub>)<sub>2</sub>,<sup>46</sup> respectively. Furthermore, polymers **3a** and **4a** show peak positions very similar to their monomeric analogues. This shows that the coordination sphere of the iron metal is relatively unperturbed by polymerization. Variations in the extinction coefficients of compounds **3a** and **4a** can be attributed to the inaccuracies of the molecular weights that are inherent to polymers.

Figure 4 shows some of the molecular orbitals of **1a** and **1b** involved in the transition with the largest calculated oscillator strength (549 nm), which can be described as a shift of the electron density from the HOMO–2, HOMO–1, and HOMO orbitals, terminating on the LUMO, LUMO+1, LUMO+2, and LUMO+5 orbitals. Because the transition involves a net electron shift from the iron to the Terpy ligand, this is consistent with the assignment of MLCT. A similar transition was calculated for complexes **2a** and **2b** at 572 nm. A number of low-intensity transitions at lower energies were also calculated for both complexes, corresponding to the shoulders observed at ca. 620 nm in the absorption spectra in Figure 3.

**Vibrational Spectroscopy.** FT-IR spectra are dominated by aromatic ring deformations and anionic vibrations. Solid-state rR was employed to specifically investigate the behavior of the FeTerpy center as a function of the temperature. rR is well suited to this because it shows selective enhancement of the modes within active chromophores, where the excitation wavelength ( $\lambda_{ex}$ ) determines which particular chromophore is being probed.<sup>36</sup> rR spectra were collected at  $\lambda_{ex}$  568 (exciting the MLCT); see Figure 5. Because rR spectroscopy is biased toward the detection of electronically active regions, compounds with similar chromophores (**1a/3a** and **2a/4a**) show only minor spectral differences. This is consistent with the coordination environments being unperturbed during polymerization. Furthermore, vibrations of the counterions are no longer observed because they do not take part in electronic excitation. By comparison to DFT models, the enhanced vibrational modes were found to primarily consist of Terpy ring distortions. Significant activity of the chelating nitrogen atoms was observed, which is consistent with the assignment of the electronic transitions as MLCT. Peak assignments and example vibrational modes are included in the Supporting Information (Tables S4.1 and S4.2 and Figure S4.3).

The spectra were recorded at 79, 298, and 362 K. No changes in the vibrational modes were observed, suggesting the absence of SCO within this temperature range.

**Magnetic Susceptibility.** The TD magnetic susceptibilities of compounds **1a**, **1b**, **2a**, **2b**, **3a**, and **4a** were performed for heating from 4.5 to 300 K (350 K for **2b**). Both **1a** and **1b** had magnetic moments of 1.35  $\mu_B$  (**1a**) and 0.90  $\mu_B$  (**1b**) for all measured temperatures within the range of literature values for LS complexes (see the Supporting Information).<sup>3,47,48</sup> **2a** remains LS for all measured temperatures; however, when **2b** is heated beyond 294 K, the start of an SCO curve is observed (Figure 6). The equipment limitations prevent the full curve from being observed. These LS magnetic moment values, which originate primarily from second-order Zeeman effects for the



**Figure 3.** Electronic absorption spectra. Left: **1a**, **1b**, **2a**, and **2b** recorded at  $10^{-5}$  M in acetonitrile. Right: **3a** and **4a** recorded at  $10^{-5}$  M in chloroform.

**Table 3.** MLCT Absorption Peak Wavelengths and Extinction Coefficients

complex	$\lambda_{\max}/\text{nm}$ ( $\epsilon/10^3 \text{ L mol}^{-1} \text{ cm}^{-1}$ )
$[\text{Fe}(\text{Terpy})_2](\text{ClO}_4)_2$	552 <sup>45</sup>
$[\text{Fe}(\text{PhTerpy})_2](\text{ClO}_4)_2$	566 <sup>46</sup>
<b>1a</b>	550 (12)
<b>1b</b>	550 (12)
<b>2a</b>	567 (29)
<b>2b</b>	567 (30)
<b>3a</b>	555 (12)
<b>4a</b>	567 (26)

$t_{2g}^6 (^1A_{1g})$  states, are in accordance with the crystallographic Fe–N bond lengths and, below, with the Mössbauer parameters. A structural determination at 400 K or above would help substantiate the SCO in **2b**.

Compounds **3a** and **4a** both show evidence of a paramagnetic impurity. This is a regular occurrence with postsynthetic modifications of PP, in which trace amounts of unreacted phenols could be trapped in the polymer matrix, potentially reacting with the iron. In addition, iron may have coordinated to the PP backbone,<sup>9</sup> or during the course of the reaction, iron(II) could have been oxidized to iron(III).

**Mössbauer Spectroscopy.** As a final means of investigating the coordination mode and spin state of the complexes, variable-temperature Mössbauer spectroscopy was employed.

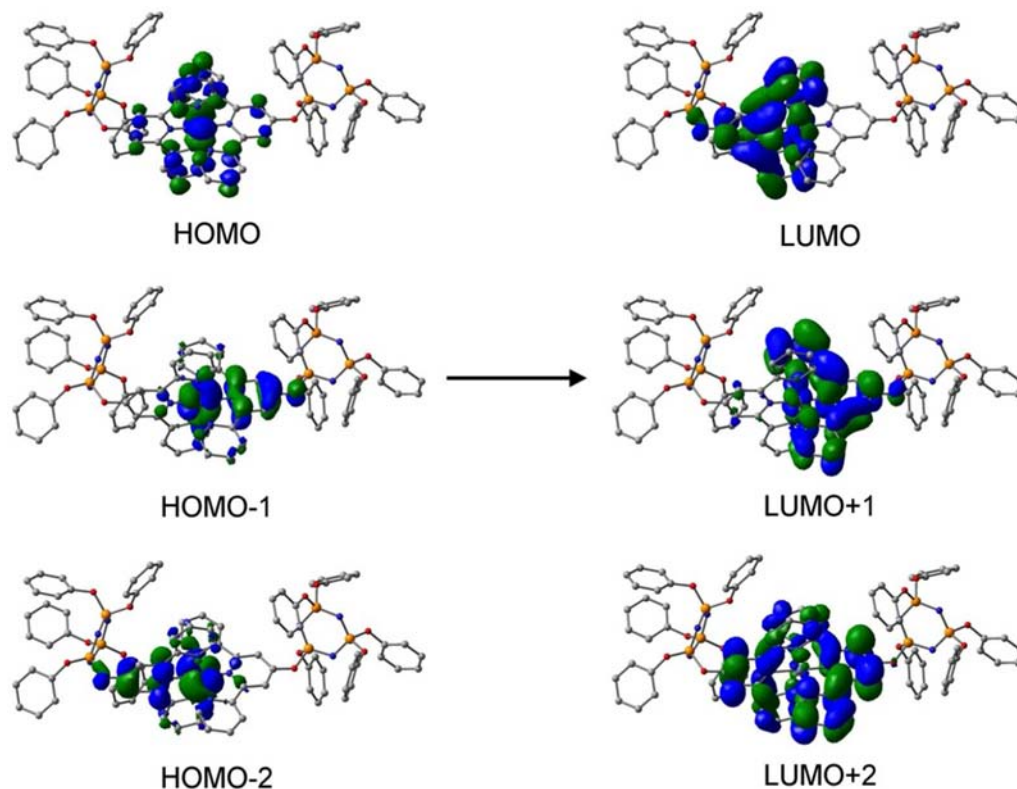


**Figure 4.** Molecular orbitals associated with the 549 nm transition.

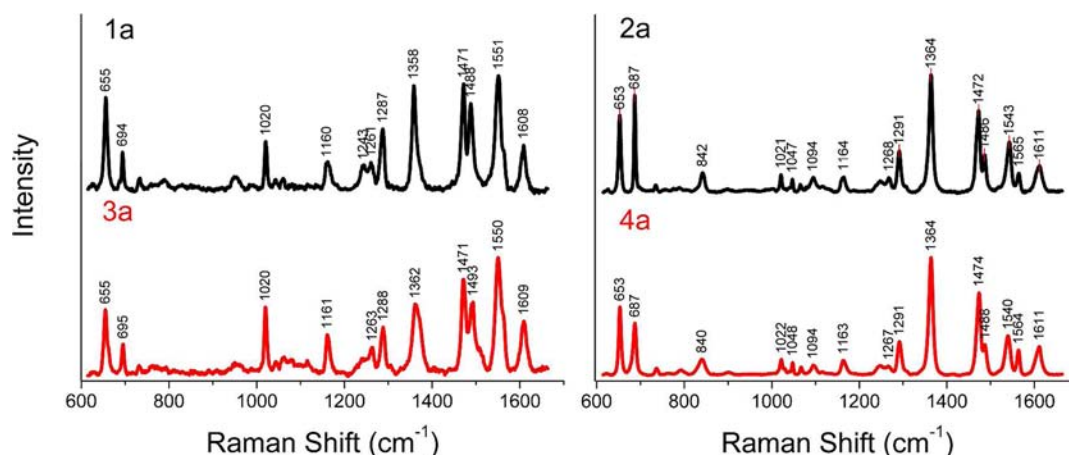


Figure 5. Solid-state rR spectra recorded using 568 nm excitation.

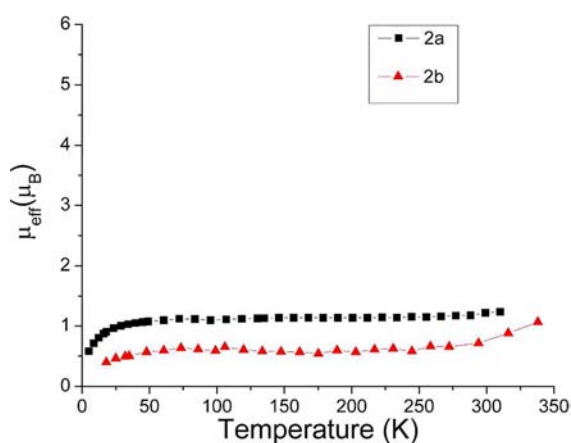


Figure 6. Magnetic moments of 2a and 2b.

Natural abundance iron provided an acceptable signal-to-noise ratio for the small-molecule complexes **1a** and **2a**. However, because the polymeric complexes **3a** and **4a** contained less iron per volume, enriched  $^{57}\text{Fe}$  was required to obtain acceptable data. Spectra were recorded at 4.7 and 293 K (see Table S7.1 in the Supporting Information for a summary of Mössbauer data).

**1a** ( $\delta = 0.27 \text{ mm s}^{-1}$ ;  $\Delta E_{\text{Q}} = 0.96 \text{ mm s}^{-1}$ ) and **2a** ( $\delta = 0.24 \text{ mm s}^{-1}$ ;  $\Delta E_{\text{Q}} = 0.98 \text{ mm s}^{-1}$ ) both displayed nearly symmetrical quadrupole doublets consistent with a single LS  $\text{Fe}^{\text{II}}\text{Terpy}_2$  species for all measured temperatures consistent with the other data collected. The parameters are very similar to comparable Terpy-based iron(II) complexes previously measured.<sup>49–53</sup> This invariance in the parameters suggests that the R group (a phosphazene in this case) at the back of the Terpy ligand does not strongly influence the ligand field of the Terpy-bound iron.

Spectra of **3a** indicated the presence of a LS  $\text{Fe}^{\text{II}}\text{Terpy}_2$  species analogous to that of **1a**; however, an intermediate-relaxing paramagnetic impurity was also observed (see Figure 7). This species was observable in the Mössbauer spectrum as a broad sextet, which has relaxed partially into what can be fitted as a quadrupole doublet. The isomer shift of this species ( $\delta = 0.5 \text{ mm s}^{-1}$ ), quadrupole splitting ( $\Delta E_{\text{Q}} = 0.45 \text{ mm s}^{-1}$ ), and magnetic hyperfine field of the slow-relaxing form ( $B_{\text{int}} = 55 \text{ T}$ ) all suggest that this is HS iron(III).<sup>54,55</sup> Polymers are, of course, a distribution of products rather than one pure species, and it is likely other iron species are present, e.g., coordination to

nonspecific sites in the polymer matrix. Reducing the relative amount of iron added to the polymer reduced the presence of this species but did not eliminate it.

The Mössbauer spectrum of **4a** was complicated by the presence of multiple species. A quadrupole doublet corresponding to approximately 20% of the total iron indicated the presence of the Terpy-bound complex, analogous to **2a**. A second quadrupole doublet was indicative of HS iron(II), and the intermediate-relaxing HS iron(III) species seen in **3a** was also present and in similar amounts.

## CONCLUSIONS

New CTP ligands  $\text{L}^1$  and  $\text{L}^2$  and PP ligands  $\text{L}^{1\text{P}}$  and  $\text{L}^{2\text{P}}$  have been prepared from the reaction of sodium salts of the hydroxyl species HOTerpy or HOPHTerpy with the appropriate CTP or PP precursor. Complexes **1a**, **1b**, **2a**, **2b**, **3a**, and **4a** were synthesized by reacting 2 equiv of the respective ligand with 1 equiv of either iron perchlorate or iron chloride followed by an anion metathesis. All small-molecule compounds were characterized by  $^{31}\text{P}$  and  $^1\text{H}$  NMR, ESI-MS, and elemental analysis. All polymeric compounds were characterized by  $^{31}\text{P}$  and  $^1\text{H}$  NMR, elemental analysis, DSC, and gel permeation chromatography. Three of the compounds (**1a**, **1b**, and **2b**) were characterized by X-ray crystallography and were shown to have the expected  $[\text{Fe}(\text{RTerpy})_2]^{2+}$  structure with a “ $\text{N}_6$ ” coordination sphere. Using electronic absorption and solid-state rR and Mössbauer spectroscopy, it was determined that the polymeric species were coordinating to iron in the same way as small-molecule species. The TD-DFT results show that attachment of the Terpy unit directly to the phosphazene gives small interactions between the phosphazene and Terpy, although they are primarily localized to the geminal phosphorus atom. By the addition of the phenyl spacer that remains out-of-plane with the aromatic ligand, those small interactions were eliminated. This is particularly useful for the future design of systems; by including a phenyl spacer, the physical properties of a group can remain unaffected by the phosphazene. For all OTerpy-based complexes reported here, the spin state remains LS; however, for the small-molecule OPhTerpy complexes, SCO starts beyond 300 K, suggesting that, by the appropriate selection of the coordination site, it may be possible to graft a functional SCO group to a PP.

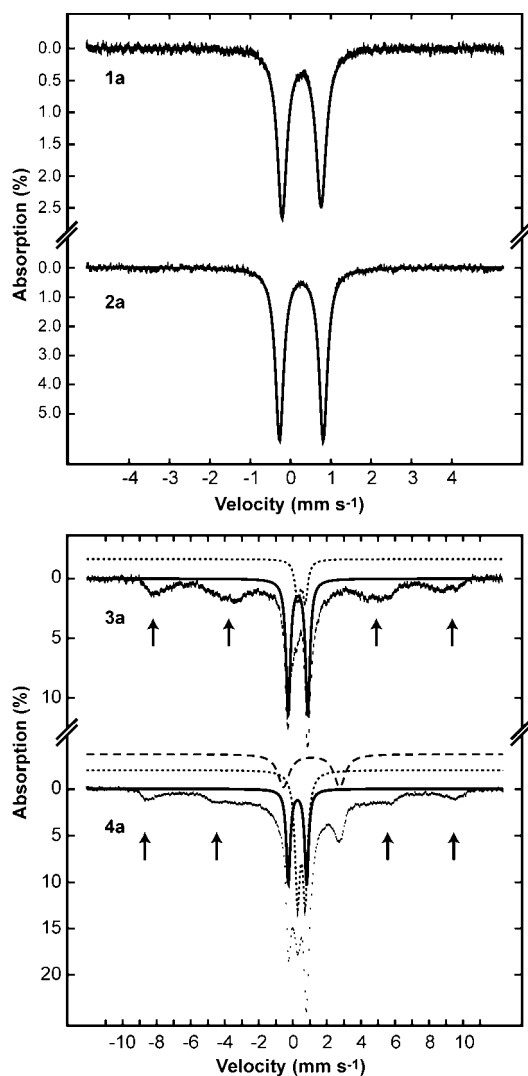


**Figure 7.** Mössbauer spectra of **1a**, **2a**, **3a**, and **4a** measured at 4.7 K and with a magnetic field of 47 mT applied parallel to the  $\gamma$ -rays. **1a** and **2a** exhibit almost symmetrical quadrupole doublets, which can be fitted (solid lines through data). **3a** and **4a** can be deconvoluted into several subspectra; a quadrupole doublet with the same parameters as those exhibited by the parent compound (solid line) and an intermediate-relaxing HS iron(III) species (arrows and dotted line). In addition, the spectrum of **4a** shows a quadrupole doublet consistent with HS iron(II) (dashed lines).

## ■ ASSOCIATED CONTENT

### Supporting Information

Crystallographic information files (CIF) for compounds **1a**·CH<sub>3</sub>CN, **1b**·CH<sub>3</sub>CN, and **2b**, selected bond parameters, spectral data, TD-DFT data, and vibrational mode assignments. This material is available free of charge via the Internet at <http://pubs.acs.org>.

## ■ AUTHOR INFORMATION

### Corresponding Author

\*E-mail: [e.ainscough@massey.ac.nz](mailto:e.ainscough@massey.ac.nz) (E.W.A.), [a.brodie@massey.ac.nz](mailto:a.brodie@massey.ac.nz) (A.M.B.).

### Notes

The authors declare no competing financial interest.

## ■ ACKNOWLEDGMENTS

We thank Assoc. Prof. S. Telfer and the MacDiarmid Institute for Advanced Materials and Nanotechnology for the use of the Spider diffractometer, the Best-Grid super computer for the use of the supercomputer, Dr. Matthias Lein for the use of the double-helix super computer and the use of *Gaussian09*, and Associate Prof. A. Partridge for the use of *GaussView* and gratefully acknowledge financial support from the Massey University Research Fund and the Massey University Ph.D. scholarship (to R.J.D.). We also thank G. Weal for help in collecting the Mössbauer data.

## ■ REFERENCES

- (1) Kahn, O.; Martinez, C. J. *Science* **1998**, *279*, 44.
- (2) Gutlich, P.; Goodwin, H. A. *Spin Crossover in Transition Metal Compounds I*; Springer: New York, 2004; Vol. 233, p 1.
- (3) Kitchen, J. A.; White, N. G.; Gandolfi, C.; Albrecht, M.; Jameson, G. N. L.; Tallon, J. L.; Brooker, S. *Chem. Commun.* **2011**, *46*, 6464.
- (4) Roubeau, O.; Natividad, E.; Agricole, B.; Ravaine, S. *Langmuir* **2007**, *23*, 3110.
- (5) Boillot, M. L.; Sour, A.; Delhaes, P.; Mingotaud, C.; Soyer, H. *Coord. Chem. Rev.* **1999**, *192*, 47.
- (6) Letard, J. F.; Nguyen, O.; Soyer, H.; Mingotaud, C.; Delhaes, P.; Kahn, O. *Inorg. Chem.* **1999**, *38*, 3020.
- (7) Djukic, B.; Dube, P. A.; Razavi, F.; Seda, T.; Jenkins, H. A.; Britten, J. F.; Lemaire, M. T. *Inorg. Chem.* **2009**, *48*, 699.
- (8) Chandrasekhar, V.; Thilagar, P.; Pandian, B. M. *Coord. Chem. Rev.* **2007**, *251*, 1045.
- (9) Kirk, S. *Cyclo- and Polyphosphazenes Containing 2-Oxypyridine Moieties Coordinated to Selected Transition Metals*; Massey University: Palmerston North, New Zealand, 2008.
- (10) Ainscough, E. W.; Brodie, A. M.; Chaplin, A. B.; O'Connor, J. M.; Otter, C. A. *Dalton Trans.* **2006**, 1264.
- (11) Diaz, C.; Izquierdo, I. *Polyhedron* **1999**, *18*, 1479.
- (12) Ainscough, E. W.; Allcock, H. R.; Brodie, A. M.; Gordon, K. C.; Hindenlang, M. D.; Horvath, R.; Otter, C. A. *Eur. J. Inorg. Chem.* **2011**, 3691.
- (13) Diefenbach, U.; Cannon, A. M.; Stromburg, B. E.; Olmeijer, D. L.; Allcock, H. R. *J. Appl. Polym. Sci.* **2000**, *78*, 650.
- (14) Carriedo, G. A.; Alonso, F. J. G.; Soto, A. P. *J. Inorg. Organomet. Polym.* **2007**, *17*, 399.
- (15) Spitaleri, A.; Pertici, P.; Scalera, N.; Vitulli, G.; Hoang, M.; Turney, T. W.; Gleria, M. *Inorg. Chim. Acta* **2003**, *352*, 61.
- (16) Diaz, C.; Valenzuela, M. L.; Spodine, E.; Moreno, Y.; Pena, O. *J. Cluster Sci.* **2007**, *18*, 831.
- (17) Diaz, C.; Castillo, P. *Polym. Bull.* **2003**, *50*, 123.
- (18) Carriedo, G. A.; Presa, A.; Valenzuela, M. L.; Ventalon, M. J. *Organomet. Chem.* **2009**, *694*, 249.
- (19) Carriedo, G. A.; Alonso, F. J. G.; Gonzalez, P. A.; Valenzuela, C. D.; Saez, N. Y. *Polyhedron* **2002**, *21*, 2579.
- (20) Carriedo, G. A.; Alonso, F. J. G.; Gonzalez, P. A.; Gomez-Elipe, P. *Polyhedron* **1999**, *18*, 2853.
- (21) Allcock, H. R.; Lavin, K. D.; Tollefson, N. M.; Evans, T. L. *Organometallics* **1983**, *2*, 267.
- (22) Beves, J. E.; Dunphy, E. L.; Constable, E. C.; Housecroft, C. E.; Kepert, C. J.; Neuburger, M.; Price, D. J.; Schaffner, S. *Dalton Trans.* **2008**, 386.
- (23) Lee, Y. H.; Ohta, A.; Yamamoto, Y.; Komatsu, Y.; Kato, K.; Shimizu, T.; Shinoda, H.; Hayami, S. *Polyhedron* **2011**, *30*, 3001.
- (24) Zhang, W.; Zhao, F.; Liu, T.; Yuan, M.; Wang, Z. M.; Gao, S. *Inorg. Chem.* **2007**, *46*, 2541.
- (25) Constable, E. C.; Ward, M. D. *J. Chem. Soc., Dalton Trans.* **1990**, 1405.
- (26) Spahni, W.; Calzaferri, G. *Helv. Chim. Acta* **1984**, *67*, 450.
- (27) McBee, E. T.; Okuhara, K.; Morton, C. J. *Inorg. Chem.* **1966**, *5*, 450.
- (28) Akermark, B.; Vitagliano, A. *Organometallics* **1985**, *4*, 1275.

(29) Allcock, H. R. *Chemistry and Applications of Polyphosphazenes*; John Wiley & Sons Inc.: Hoboken, NJ, 2003.

(30) Sheldrick, G. M. *SHELXL: Suite of Programs for Crystal Structure Analysis*; University of Gottingen: Gottingen, Germany, 1998.

(31) Dolomanov, O. V.; Bourhis, L. J.; Gildea, R. J.; Howard, J. A. K.; Puschmann, H. J. *Appl. Crystallogr.* **2009**, *42*, 339.

(32) Vandersluis, P.; Spek, A. L. *Acta Crystallogr., Sect. A* **1990**, *46*, 194.

(33) Dolomanov, O. V. *CHN*, 1.0 ed.; The University of Nottingham: Nottingham, 2004.

(34) Lundin, N. J.; Walsh, P. J.; Howell, S. L.; McGarvey, J. J.; Blackman, A. G.; Gordon, K. C. *Inorg. Chem.* **2005**, *44*, 3551.

(35) Howell, S. L.; Matthewson, B. J.; Polson, M. I. J.; Burrell, A. K.; Gordon, K. C. *Inorg. Chem.* **2004**, *43*, 2876.

(36) Horvath, R.; Gordon, K. C. *Coord. Chem. Rev.* **2010**, *254*, 2505.

(37) Frisch, M. J.; Trucks, G. W.; Schlegel, H. B.; Scuseria, G. E.; Robb, M. A.; Cheeseman, J. R.; Scalmani, G.; Barone, V.; Mennucci, B.; Petersson, G. A.; Nakatsuji, H.; Caricato, M.; Li, X.; Hratchian, H. P.; Izmaylov, A. F.; Bloino, J.; Zheng, G.; Sonnenberg, J. L.; Hada, M.; Ehara, M.; Toyota, K.; Fukuda, R.; Hasegawa, J.; Ishida, M.; Nakajima, T.; Honda, Y.; Oaaa, K.; Nakai, H.; Vreven, T.; Montgomery, J. A., Jr.; Peralta, J. E.; Ogliaro, F.; Bearpark, M.; Heyd, J. J.; Brothers, E.; Kudin, K. N.; Staroverov, V. N.; Kobayashi, R.; Normand, J.; Raghavachari, K.; Rendell, A.; Burant, J. C.; Iyengar, S. S.; Tomasi, J.; Cossi, M.; Rega, N.; Millam, J. M.; Klene, M.; Knox, J. E.; Cross, J. B.; Bakken, V.; Adamo, C.; Jaramillo, J.; Gomperts, R.; Stratmann, R. E.; Yazyev, O.; Austin, A. J.; Cammi, R.; Pomelli, C.; Ochterski, J. W.; Martin, R. L.; Morokuma, K.; Zakrzewski, V. G.; Voth, G. A.; Salvador, P.; Dannenberg, J. J.; Dapprich, S.; Daniels, A. D.; Farkas, Ö.; Foresman, J. B.; Ortiz, J. V.; Cioslowski, J.; Fox, D. J. *Gaussian 09*, A.1 ed.; Gaussian, Inc.: Wallingford, CT, 2009.

(38) Dennington, R.; Keith, T.; Millam, J. *GaussView*, 5th ed.; Semichem Inc.: Shawnee Mission, KS, 2009.

(39) Alver, O.; Parlak, C.; Senyel, M. *J. Mol. Struct.* **2009**, *923*, 120.

(40) Tantirungrotechai, Y.; Phanasant, K.; Roddecha, S.; Surawatanawong, P.; Sutthikhum, V.; Limtrakul, J. *J. Mol. Struct.* **2006**, *760*, 189.

(41) Murguly, E.; Norsten, T. B.; Branda, N. *J. Chem. Soc., Perkin Trans. 2* **1999**, 2789.

(42) Hughes, M. C.; Macero, D. J.; Rao, J. M. *Inorg. Chim. Acta* **1981**, *49*, 241.

(43) Rao, J. M.; Hughes, M. C.; Macero, D. J. *Inorg. Chim. Acta* **1976**, *16*, 231.

(44) Rao, J. M.; Macero, D. J.; Hughes, M. C. *Inorg. Chim. Acta* **1980**, *41*, 221.

(45) Fordsmith, M.; Sutin, N. *J. Am. Chem. Soc.* **1930**, *1961*, 83.

(46) McMurtrie, J.; Dance, I. *Cryst. Eng. Commun.* **2009**, *11*, 1141.

(47) Boca, R.; Renz, F.; Boca, M.; Fuess, H.; Haase, W.; Kickelbick, G.; Linert, W.; Vrbova-Schikora, M. *Inorg. Chem. Commun.* **2005**, *8*, 227.

(48) Baker, W. A.; Bobonich, H. M. *Inorg. Chem.* **1964**, *3*, 1184.

(49) Reiff, W. M. *J. Am. Chem. Soc.* **1974**, *96*, 3829.

(50) Maeda, Y.; Ohshio, H.; Takashima, Y. *Bull. Chem. Soc. Jpn.* **1982**, *55*, 3500.

(51) Ohshio, H.; Spiering, H.; Ksenofontov, V.; Renz, F.; Gutlich, P. *Inorg. Chem.* **2001**, *40*, 1143.

(52) Hayami, S.; Kojima, Y.; Urakami, D.; Ohta, K.; Inoue, K. *Monatsh. Chem.* **2009**, *140*, 829.

(53) Hayami, S.; Urakami, D.; Kojima, Y.; Yoshizaki, H.; Yamamoto, Y.; Kato, K.; Fuyuhiko, A.; Kawata, S.; Inoue, K. *Inorg. Chem.* **2010**, *49*, 1428.

(54) Greenwood, N. N.; Gibb, T. C. *Mössbauer Spectroscopy*; Chapman and Hall Ltd.: London, 1971.

(55) Gütllich, E. B.; Trautwein, A. X. *Mössbauer Spectroscopy and Transition Metal Chemistry*; Springer-Verlag: New York, 2011.